

A correlation method for high-frequency response of a cargo during dry transport in high seas

Vimal Vinayan* and Jun Zou^a

Houston Offshore Engineering, An Atkins Company, Houston, TX, USA

(Received October 22, 2014, Revised May 9, 2016, Accepted May 10, 2016)

Abstract. Cargo, such as a Tension Leg Platform (TLP), Semi-submersible platform (Semi), Spar or a circular Floating Production Storage and Offloading (FPSO), are frequently dry-transported on a Heavy Lift Vessel (HLV) from the point of construction to the point of installation. The voyage can span months and the overhanging portions of the hull can be subject to frequent wave slamming events in rough weather. Tie-downs or sea-fastening are usually provided to ensure the safety of the cargo during the voyage and to keep the extreme responses of the cargo, primarily for the installed equipment and facilities, within the design limits. The proper design of the tie-down is dependent on the accurate prediction of the wave slamming loads the cargo will experience during the voyage. This is a difficult task and model testing is a widely accepted and adopted method to obtain reliable sea-fastening loads and extreme accelerations. However, it is crucial to realize the difference in the inherent stiffness of the instrument that is used to measure the tri-axial sea fastening loads and the prototype design of the tie-downs. It is practically not possible to scale the tri-axial load measuring instrument stiffness to reflect the real tie-down stiffness during tests. A correlation method is required to systematically and consistently account for the stiffness differences and correct the measured results. Direct application of the measured load tends to be conservative and lead to over-design that can reflect on the overall cost and schedule of the project. The objective here is to employ the established correlation method to provide proper high-frequency responses to topsides and hull design teams. In addition, guidance for optimizing tie-down design to avoid damage to the installed equipment, facilities and structural members can be provided.

Keywords: wave slamming; impulsive response function; sea-fastening; high-frequency responses; dry transport; optimization of tie-down design and correlation method

1. Introduction

The dry transport of an offshore platform by a Heavy Lift Vessel (HLV) is a typical option used by the offshore industry to ferry the hull from the construction yard to a near-shore location. A typical HLV-Cargo combination is shown in Fig. 1 and it can be seen that the Cargo is near sea level and has overhanging portions on both sides of the HLV. The whole voyage may take several months and the metocean criteria along the route can be significantly severe than the metocean criteria in-site. The overhanging portions of the Cargo will experience both horizontal and vertical

*Corresponding author, Ph.D., E-mail: vvinayan@houston-offshore.com

^a Ph.D., E-mail: jzou@houston-offshore.com

slamming loads, large rotational motion and extreme accelerations during the long journey. These loads and motions can be such that design governing cases for topsides and hull local structure might occur during the dry transportation stage. Hence, it is crucial to simulate the dynamic response of the Cargo accurately and consistently to ensure a safe and robust design.

In order to prevent the Cargo from possible shifting, lifting and overturning on the HLV, tie-downs are widely employed to ensure that the extreme responses of the Cargo are within the design limits. Horizontal tie-downs, when used, prevent the Cargo from sliding or overturning on the HLV deck. Vertical tie-downs that prevent the Cargo from lifting or overturning are seldom used as they can cause structural damage to the deck of the HLV and lead to catastrophic failure.

Since wave slamming loads are impulsive in nature and last only for a short duration of time, they are extremely difficult to predict accurately by numerical simulation. Model testing to measure wave slamming loads is a widely accepted industry practice. However, it is essential to understand the limits of model testing, to identify the differences between the model and prototype scales, to correlate the measured results with prototype problems and to apply the measured results in design correctly.

2. Model testing

A typical model-test setup is illustrated in Fig. 2 for a dry transport test. Fig. 2(a) is an elevation view, Fig. 2(b) is the top view and Fig. 2(c) is the blow-up view of the tri-axial load cells installed on model. The tri-axial loads cells, highlighted in red in Figs. 2(a) and 2(b), connect the Cargo and the HLV, and measure the sea-fastening loads in the X, Y and Z directions. As shown in Fig. 2(b), there are four sets of tri-axial load cells from which the resultant overturning moments can be derived. The other instruments that are used during the model test are:

- a) Accelerometers to measure the accelerations;
- b) Motion tracking system to measure the combined six degree-of-freedom motions;
- c) Pressure patches affixed on the different parts of the cargo to measure the slamming pressures;
- d) Wave elevation probes that measure the relative position of the cargo with respect to the wave surface.

The model test setup shown in Fig. 2 can be represented by numerical models shown in Fig. 3. The dynamic response of a dry transport model test configuration to impulse loads is crucial towards determining the accuracy or usefulness of the measured forces or accelerations. This is so because the inherent characteristics of the measurement system, i.e., its stiffness (the tri-axial load cells along with the connection accessories act as a spring) and damping values, tied to the mass of the cargo, determine the natural period of the response and the dynamic amplification of the measured values.

A common error in employing the model test results for design is to directly apply the measured data without knowing the differences between the model and prototype scales. Due to the limits of model test setup, the stiffness of commercial tri-axial load cells cannot properly represent the stiffness of prototype tie-downs. In addition, the rigidness of Cargo and HLV mode cannot be scaled accurately from prototype Cargo and HLV. It is crucial to recognize these differences and develop a correlation method to employ the measured results correctly and consistently to maximize the value of model testing.

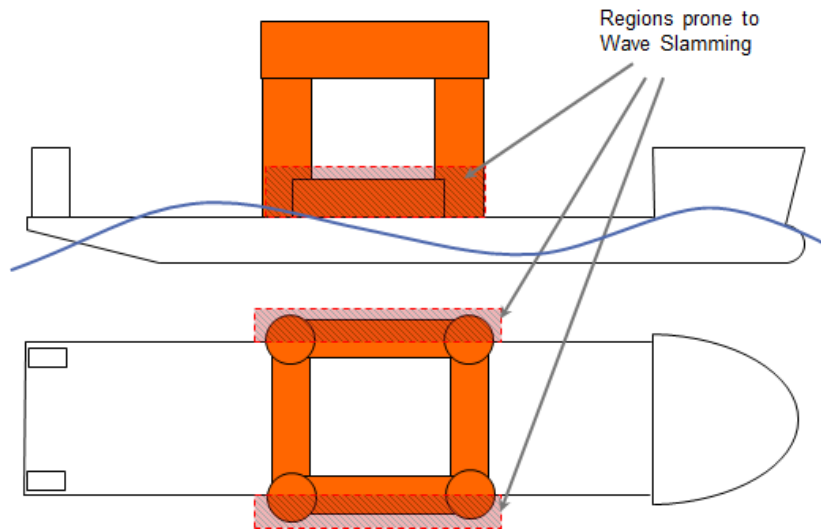
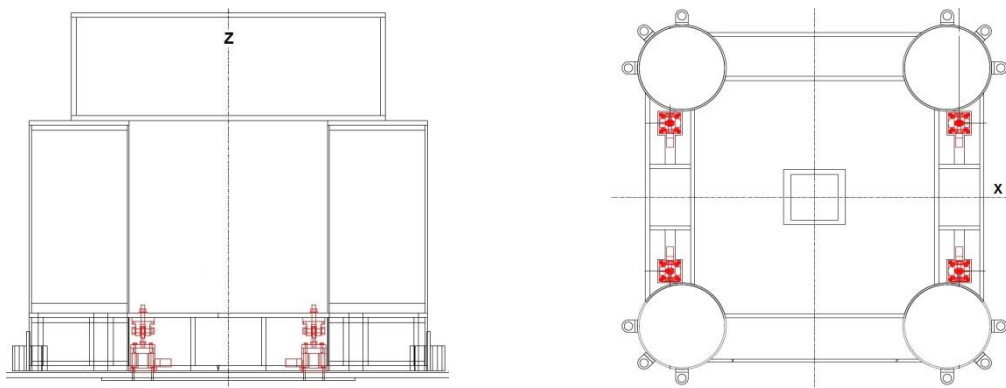
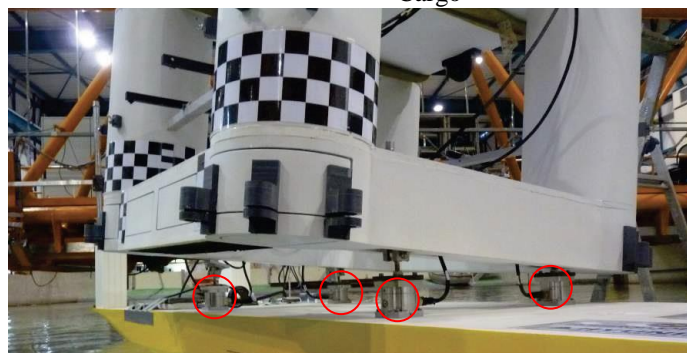


Fig. 1 Dry transport of an floating platform on a Heavy-Lift Vessel (H LV)



(a) Elevation view of tri-axial load cells linked between Cargo and HLV
 (b) Top view of tri-axial load cells locations on Cargo



(c) Blown up view prior to attachment of cargo to HLV in model test (load-cells shown in red circles)

Fig. 2 Dry transport model test setup

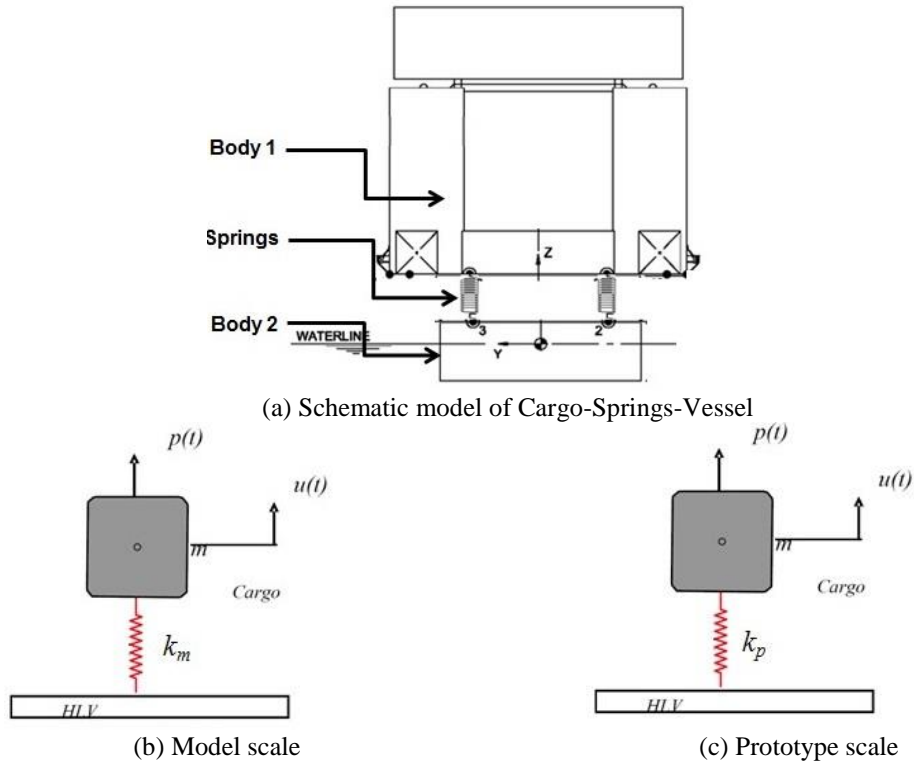


Fig. 3 Representations of dry transport in the model test and numerical simulations

3. Numerical model

The main aim of conducting a dry-transport model test campaign is to determine the factors of safety against uplift and overturning. In the absence of sea-fastening, the weight of the cargo is the governing factor that determines the possibility of uplift and overturning. The decision to include sea-fastening is made if sufficient factor of safety against uplift and overturning is not available.

The reaction loads measured by the tri-axial load cells during the model tests represent the resultant of the overall loads acting on the cargo. The overall loads include – inertia loads, wave loads (including slamming) and buoyancy loads. For the purposes of calibration, a simple relation of the global equations of motions can be developed based on the model test setup. From the dry-transport model test results, it was observed that the maximum wave loading on the overhanging portion of the hull occurred in beam sea conditions (90° wave heading, see Fig. 4). For the beam sea conditions, the equations of motion of the cargo can be written as

$$\sum L_{iy} + F_y = ma_y + mgs_x \quad (1)$$

$$\sum L_{iz} + F_z = ma_z + mgc_x c_y \quad (2)$$

$$(L_{1z} + L_{2z} - L_{3z} - L_{4z})b + M_z = I_{xx}\ddot{\theta} - ma_y\overline{PG} \quad (3)$$

Eqs. (1) and (2) represent sway and heave motions. Eq. (3) is the summation of the roll moments about point P .

Here,

- (i) L_{iy} and L_{iz} ($i=1,2,3,4$) are the instantaneous reaction loads measured by the tri-axial load cells in the local vessel fixed y and z directions.
- (ii) F_y and F_z are the instantaneous fluid loads acting on the cargo. M_x is the resultant roll moment (about P). Note that these represent the wave (including slamming) and buoyancy loads in a *lumped* manner.
- (iii) a_y and a_z are the instantaneous accelerations at the center of gravity (G) of the cargo, as measured by accelerometers (accelerations including the effects of gravity).
- (iv) m is the mass of the cargo.
- (v) $s_x = \sin \theta$, $c_x = \cos \theta$ and $c_y = \cos \phi$ where θ and ϕ are the instantaneous roll and pitch angles.
- (vi) I_{xx} is the roll mass moment of inertia of the cargo (about G).
- (vii) g is the acceleration due to gravity.
- (viii) b is the transverse spacing between the tri-axial load cells.

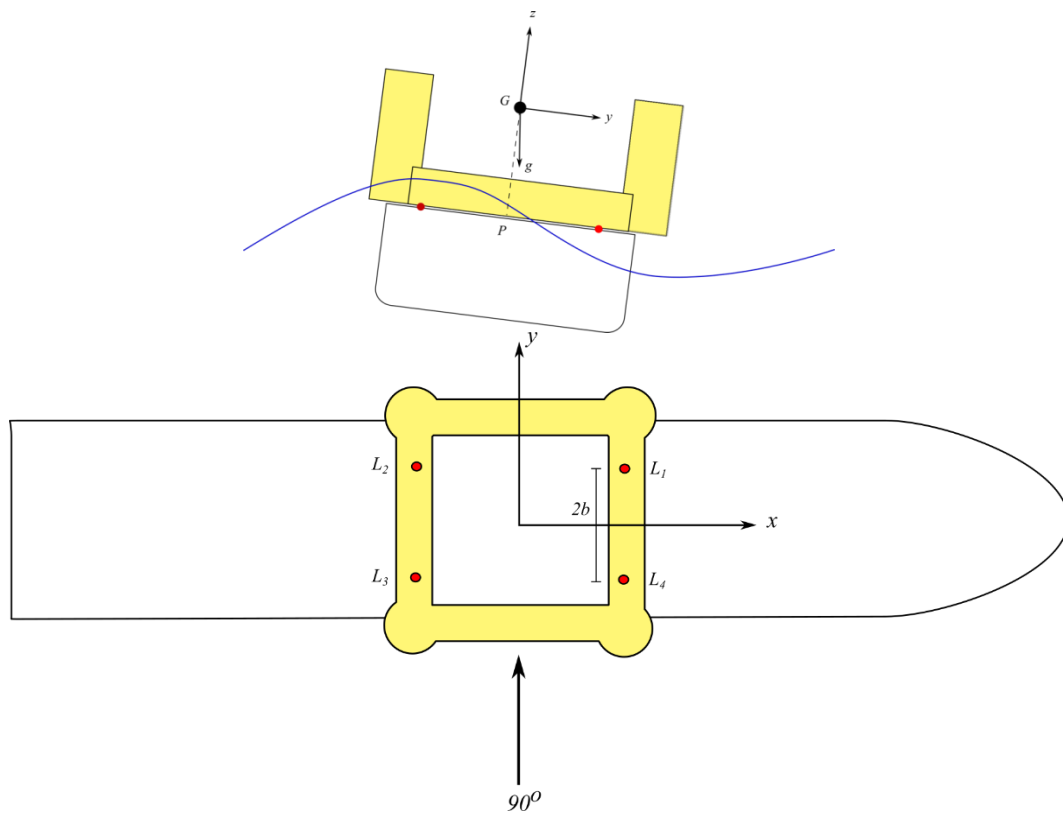


Fig. 4 HLV-Cargo global loads

In the model test setup, a small gap between the cargo and the HLV is provided to account for the height of the cribbage provided during the actual transport. With this gap, the frictional effects which do not scale correctly between prototype and model scales, can be neglected. In the model tests, the instantaneous sea-fastening loads (S_x , S_y and S_z) can be written as

$$\sum L_{ix} = S_x \quad (4)$$

$$\sum L_{iy} = S_y \quad (5)$$

$$\sum L_{iz} = S_z \quad (6)$$

However, during actual dry-transport the friction between the underside of the cargo and the deck of the HLV has to be considered. With the effects of friction included, the sea-fastening loads can be written as

$$\sum L_{ix} = S_x + \mu N_x \quad (7)$$

$$\sum L_{iy} = S_y + \mu N_y \quad (8)$$

$$\sum L_{iz} = S_z \quad (9)$$

where μ is the coefficient of friction between the cargo and the HLV deck. N_x and N_y are the normal reactions related to the weight of the cargo.

The calibration/estimation of the wave loads F_y and F_z is not a trivial exercise due to the nonlinearities associated with green water effect, slamming etc. A thorough analysis of the model tests revealed that there is a strong correlation between slamming events and high-frequency loads/accelerations. In the absence of slamming, sea-fastening loads can be obtained directly from the reaction loads using Eqs. (4)-(6). A separate numerical model is needed to address the high-frequency loads measured during the slamming events. The approach presented here is based on the assumption that the duration of the slamming events is sufficiently small that it does not affect the global motions of the vessel. The pulse width of the slamming events was found to be in the range of 0.3s to 0.5s. The global motions/loads (inertia and buoyancy loads) and the high-frequency motions/loads (slamming) can effectively be decoupled. The next part of the paper describes the development of a numerical model that addresses the high-frequency component of the loads.

The arrangement (model test setup with the Cargo attached to the HLV using tri-axial load cells) has an inherent stiffness and damping that can be obtained based on the response of a hammer test (dry conditions). The equivalent stiffness in each global degree of freedom (X, Y and Z as shown in Fig. 2) and the corresponding damping can be obtained by analyzing the response of the system from a hammer test that applies an impulsive load in that particular degree of freedom.

In each of the global degrees of freedom the overall HLV-cargo model test configuration can be represented as a single-degree of freedom mass-spring-damper system as shown in Fig. 4(a). Here m is the mass of the cargo, k is the equivalent stiffness provided by the load-cells in the appropriate global degree of freedom and c is the system damping. $u(t)$ is the displacement response of the cargo to an impulse load $p(t)$. The equivalent stiffness k and the corresponding

damping c can be obtained by matching the transient and frequency response of the simplified system to that of the measured hammer test response (see Hartog 1985 and Piersol 2010) for details.

The hammer test is conducted by applying an impulsive load to the cargo in the three degrees of freedom (dry conditions). An example of the load-cell response time series obtained from a hammer test and the corresponding spectrum showing the frequency content of the measured response is shown in Fig. 5.

The overall response of the HLV-cargo model test configuration in waves can be represented as a single-degree of freedom base-excited mass-spring-damper system as shown in Fig. 4(b). Here $x(t)$ and $y(t)$ are the absolute motions of the cargo and the HLV respectively in any one global degree of freedom X, Y or Z. The equation of motion representing the above system can be written as

$$m\ddot{u} + c\dot{u} + ku = -m\ddot{y} + p(t) \tag{10}$$

where $u=x-y$ is the relative displacement between the two objects (Hartog 1985, Wirsching 2006). As explained previously, the damping c and stiffness k can be obtained from the response of a hammer test.

In the absence of any impact loads from wave slamming (that act on the cargo), the relative displacement between the two objects ($u(t)$) is negligible and the load cells primarily measure the inertial loads due to the cargo. The cargo and HLV displacements $x(t)$ and $y(t)$, and the measured inertial loads lie in the wave-frequency (WF) regime that is consistent with the wave spectra being used in the test.

During a wave-slamming event, the cargo is subject to an impulsive load that lasts only a fraction of a second and is not long enough to affect the global motion of the HLV (represented by $y(t)$, $\ddot{y}(t)$ is assumed to remain constant during the slamming event). Based on this assumption, the overall response of the system can be decomposed into two components $y(t)$ and $u(t)$. $y(t)$ represents the wave-frequency component of the response while $u(t)$ represents the high-frequency (HF) response characteristic of a system subject to impulsive loads. A quantitative representation of the HF response can be obtained by representing the HLV-cargo combination as a single degree of freedom force-excited mass-spring system as shown in Fig. 6(a).

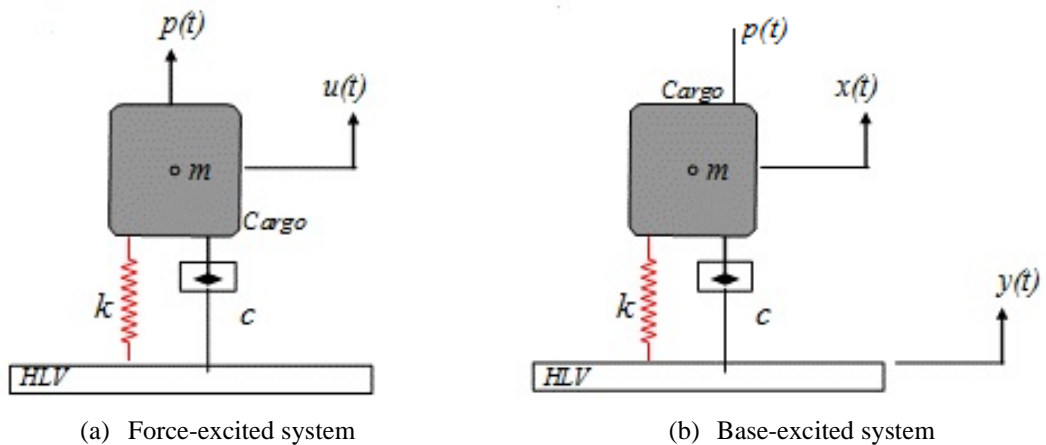
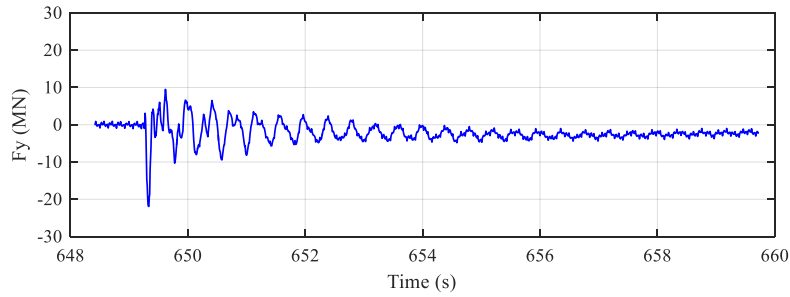
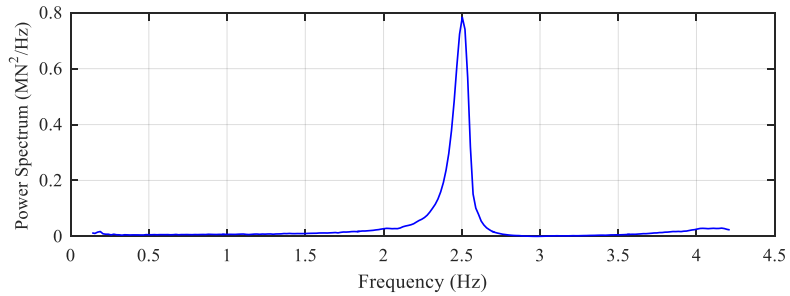


Fig. 5 Numerical representation of the model test configuration

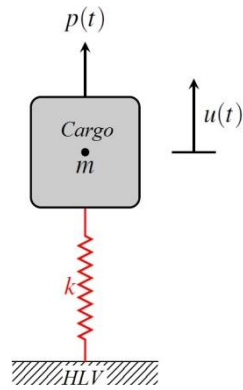


(a) Time-history of measured response

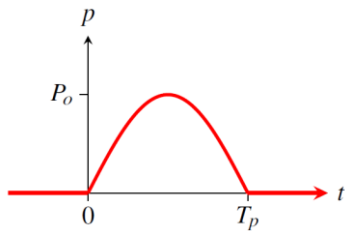


(b) Power spectrum of measured response

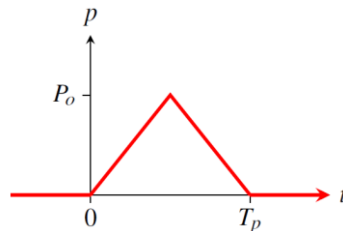
Fig. 6 Response of system from a hammer test



(a) Force-excited system



(b) Half-sine Pulse



(c) Symmetrical Triangular Pulse

Fig. 7 Representation of model test configuration and pulse form of slamming forces

The key to defining the response of the above mass-spring-damper system is to define a functional form for the wave-slammng force. Typically the external force acting on the structure due to wave slammng is represented as a half-sine pulse as shown in Fig. 6(b) or a triangular pulse as presented in Fig. 6(c) (Isaacson 1994 and Argate 2013). The results by assuming the wave slammng force to be a half-sine pulse are provided in Vinayan and Zou (2014). In this paper, formula and/or results for a triangular pulse are focused on.

For a mass-spring system subject to a symmetrical triangular pulse as shown in Fig. 5(c), the governing equation of motion is of the form (see Chopra 1995 and Piersol 2010)

$$m\ddot{u} + c\dot{u} + ku = p(t) = \begin{cases} \frac{2P_o}{T_p}t & , \quad 0 \leq t \leq T_p/2 \\ P_o - 2\frac{P_o}{T_p}\left(t - \frac{T_p}{2}\right) & , \quad T_p/2 \leq t \leq T_p \\ 0 & , \quad t \geq T_p \end{cases} \quad (11)$$

where, P_o is the maximum amplitude of the triangular pulse force excitation. T_p is the period of the pulse. The response of the system to the triangular pulse excitation can be written as

$$\frac{u(t)}{\frac{P_o}{k}} = \begin{cases} 2\left(\frac{t}{T_p} - \frac{T_n}{2\pi T_p} \sin 2\pi \frac{t}{T_n}\right) & , \quad 0 \leq t \leq T_p/2 \\ 2\left\{1 - \frac{t}{T_p} + \frac{T_n}{2\pi T_p} \left[2 \sin 2\pi \frac{(t - T_p/2)}{T_n} - \sin 2\pi \frac{t}{T_n}\right]\right\} & , \quad T_p/2 \leq t \leq T_p \\ 2\left\{\frac{T_n}{2\pi T_p} \left[2 \sin 2\pi \frac{(t - T_p/2)}{T_n} - \sin 2\pi \frac{(t - T_p)}{T_n} - \sin 2\pi \frac{t}{T_n}\right]\right\} & , \quad t \geq T_p \end{cases} \quad (12)$$

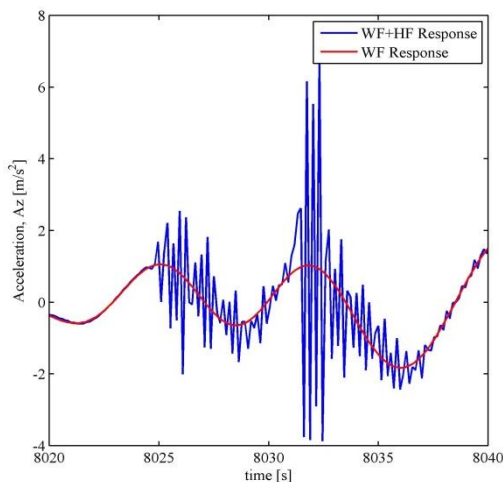
$$\frac{\ddot{u}(t)}{\frac{P_o}{k}} = \begin{cases} 2\left(\frac{T_n \omega_n^2}{2\pi T_p} \sin 2\pi \frac{t}{T_n}\right) & , \quad 0 \leq t \leq T_p/2 \\ 2\left\{\frac{T_n \omega_n^2}{2\pi T_p} \left[-2 \sin 2\pi \frac{(t - T_p/2)}{T_n} + \sin 2\pi \frac{t}{T_n}\right]\right\} & , \quad T_p/2 \leq t \leq T_p \\ 2\left\{\frac{T_n \omega_n^2}{2\pi T_p} \left[-2 \sin 2\pi \frac{(t - T_p/2)}{T_n} + \sin 2\pi \frac{(t - T_p)}{T_n} + \sin 2\pi \frac{t}{T_n}\right]\right\} & , \quad t \geq T_p \end{cases} \quad (13)$$

where it has been assumed that the system starts from rest and $T_n=2\pi/\omega_n$ is the natural period of oscillation of the system. P_o is the maximum force or amplitude of the triangular pulse slammng

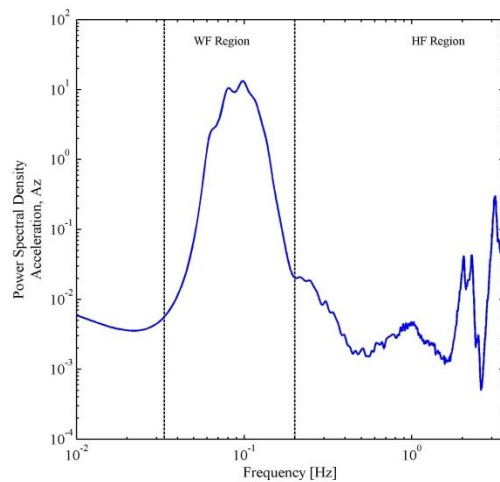
force. Note that the response in the phase $0 \leq t \leq T_p$ is that of a forced vibration, while in the phase $t \geq T_p$ is that of a free-vibration. The above set of expressions completely defines the response of a mass-spring system to a symmetrical triangular pulse that simulates a wave-slaming event. The key to understanding the transient response is to divide it into two phases (i) the forced phase that covers the response of the system within the duration of the pulse, (ii) the free-phase during which the forcing is absent and the system responds at its own natural period (T_n). In a typical model test configuration, the natural period is in the range of 0.3-0.5s or a frequency range of 2-3 Hz. Compared to the wave-frequency range normally tested, this range of frequencies falls well within the high-frequency (HF) range. The load cells and accelerometers attached to the cargo will pick up this spurious HF response.

A typical vertical acceleration response in a slamming even obtained from model tests is shown in Fig. 7. To better illustrate the high-frequency (HF) response, the wave-frequency (WF) response obtained by filtering the data (cut-off frequency = 0.2 Hz, see Fig 7(b) showing the demarcation between the WF and HF regions) is also shown superimposed on the total response. Two key observations can be made:

- The short duration over which the HF response (ringing like response) occurs: In the example shown here, the overall slamming response with both the forced and free phases occurs over a duration of 6s. This is relatively short compared to typical WF response periods. Similar HF response is seen in all the measured signals (forces and accelerations).
- The dynamic amplification of the measured response: Significant dynamic amplification of the accelerations due to the inherently high stiffness of the measurement stiffness. For example, within the slamming window shown in Fig. 7(a), the maximum WF acceleration response is about 2 m/s^2 while that of the overall response is about 6 m/s^2 . Such high accelerations are an artefact of the relatively high stiffness of the measurement system and have to be corrected before being applied for design purposes.



(a) High-frequency response measured by accelerometers



(b) Power spectrum of the overall response time-series (WF and HF regions)

Fig. 8 Response measured by sensors during a slamming event

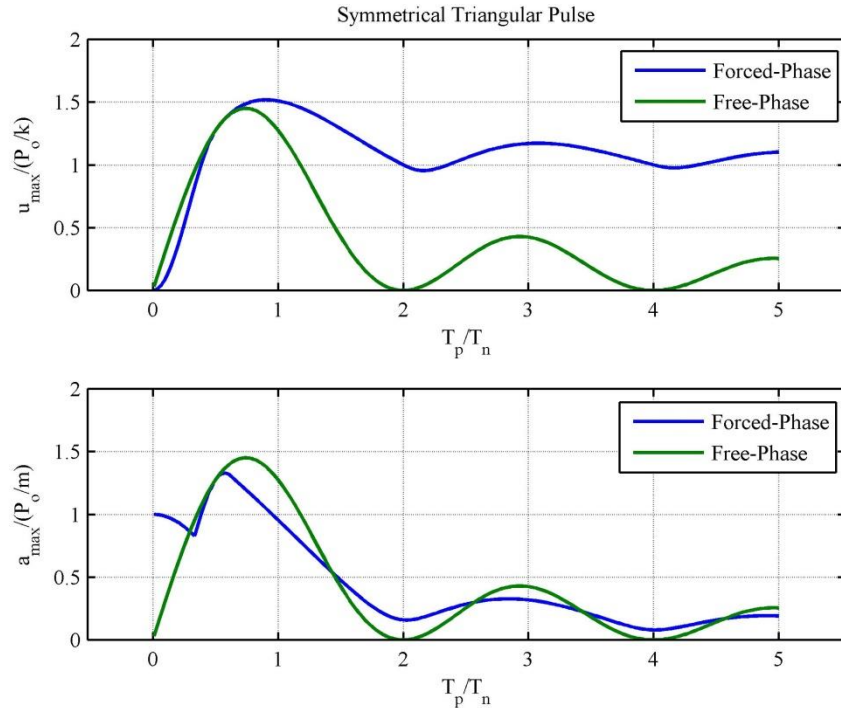


Fig. 9 Shock response spectrum from displacement (top) and acceleration (bottom) for a symmetric triangular pulse (Damping = 0%)

The underlying use of the above relations lies in developing envelope curves representing the maximum attainable displacement and acceleration as a function of T_p/T_n . This curve is useful in providing a relationship between the maximum possible displacement and acceleration for varying levels of system stiffness. Fig. 8 shows the envelope curves generated for the symmetrical triangular pulse excitation. The envelope curve is also known as the shock-response-spectrum (Chopra 1995). For a particular value of T_p/T_n , the maximum displacement or acceleration is the maximum of the free and forced vibration values.

The results presented above can be used to develop a methodology to scale the maximum acceleration experienced by the tie-down arrangement during the impulsive phase.

4. Optimization of tie-down design

In the previous section, a methodology was developed to extend the accelerations measured during a dry-transport model test to prototype scale. The extension or correlation is primarily a function of the tied-down stiffness in prototype and model scales and the pulse period (T_p) of the wave-slaming event.

During a dry transport operation, limitations are imposed on the maximum acceleration the cargo can withstand without compromising structural as well as mechanical integrity of the

onboard systems. This threshold value (a_t) consists of both the WF and HF (resulting from an impulsive wave slamming event) components. The prototype stiffness should be such that it does not amplify the HF component of the acceleration to an extent that the threshold acceleration value is exceeded. The prototype tie-down stiffness can be optimized based on this criterion.

The optimization of the tie-down design is based on the development of curves that provide a parametric representation of the ratio

$$f = \frac{a_{HFmax,p}}{a_{HFmax,m}} \quad (14)$$

as a function of the ratio of the tie-down stiffness in prototype and model scale represented as (k_p/k_m), and the pulse period (T_p). The subscripts p and m denote the prototype and model scales respectively. These curves are developed based on the detailed formulation presented in the previous section for the symmetric triangular wave-slaming pulse and are as shown in Fig. 9. Fig. 10 shows the procedure used to derive the optimum stiffness ratio.

5. Numerical results

The procedure described above can be better understood through an example, based on the acceleration response shown in Fig. 11. Within the slamming event spanning 8030 s – 8036 s, the maximum WF response is about 6.8 m/s². The corresponding filtered WF response is about $a_{WF}=1.6$ m/s² giving a maximum HF acceleration response of $a_{HFmax,m} = 5.2$ m/s² (at model scale).

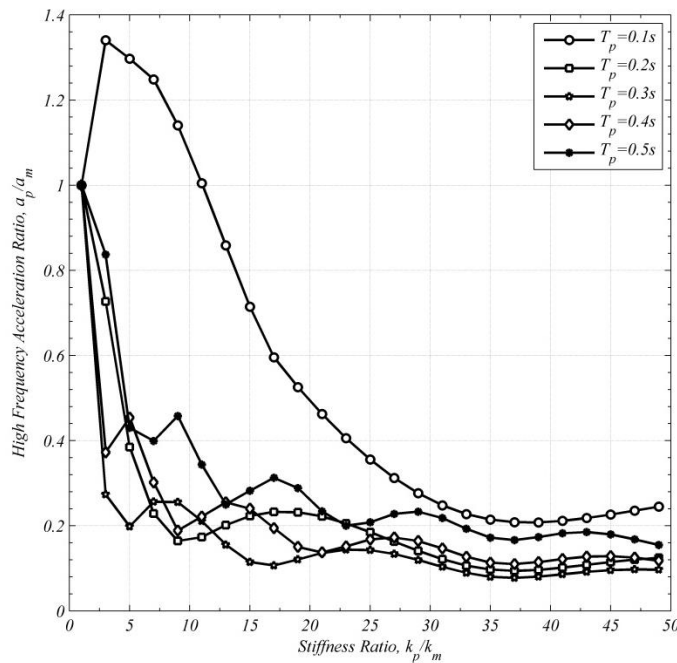


Fig. 10 Curves representing the relation between the stiffness and HF acceleration ratios for different symmetric triangular pulse periods

STEP 1:

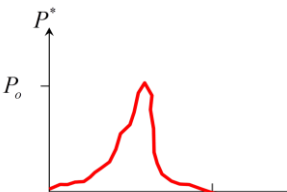
(a) Identify the instant at which the allowable threshold acceleration (a_t) is exceeded. Decompose the acceleration signal into WF (a_{WF}) and HF ($a_{HFmax,m}$) components.

(b) The maximum allowable HF acceleration in prototype scale,

$$a_{HFmax,p} = a_t - a_{WF}$$

STEP 2:

Assess the pulse period (T_p) of the slamming event by matching the impulse of the measured forces (pressure-patch measurements)

$$T_p = \frac{2}{P_0} \int_0^{t_0} P^*(t) dt$$


STEP 3:

(a) From the above steps, the pulse period (T_p) and the ratio of HF accelerations $f_{reqd} = a_{HFmax,p} / a_{HFmax,m}$ can be calculated.

(b) Obtain required stiffness ratio between prototype and model scale $r_{reqd} = k_p / k_m$

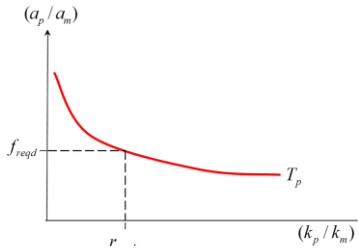


Fig. 10 Procedure to estimate the optimum stiffness ratio between prototype and model scales

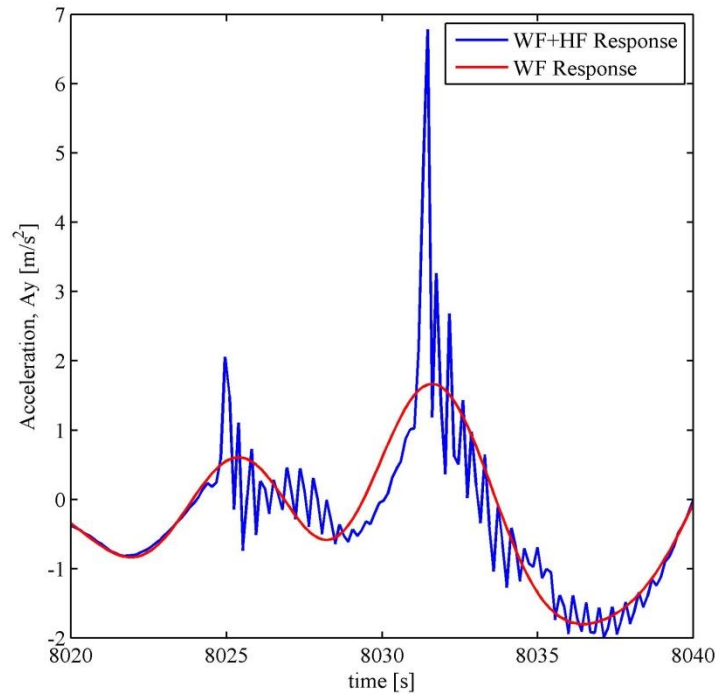


Fig. 11 High frequency (HF) response in horizontal acceleration response

The typical pulse periods of the slamming events determined based on the procedure shown in Step 2 is in the range of 0.1 s to 0.5 s. Table 1 shows the dynamic amplification associated with the acceleration response for different pulse periods. The dynamic amplification is provided for different ratios of the prototype vs model scale tie-down stiffness.

Table 1 Dynamic amplification factor for symmetric triangular pulse

k_p/k_m	Symmetrical Triangular Pulse				
	Pulse Period (s)				
	0.1	0.2	0.3	0.4	0.5
			a_p/a_m		
16	0.65	0.23	0.11	0.22	0.30
18	0.56	0.23	0.11	0.17	0.31
20	0.49	0.23	0.13	0.14	0.26
22	0.43	0.21	0.14	0.14	0.21
24	0.38	0.20	0.14	0.16	0.20
26	0.33	0.17	0.14	0.17	0.22
28	0.29	0.15	0.13	0.17	0.23
30	0.26	0.13	0.11	0.16	0.23
32	0.24	0.11	0.10	0.14	0.21
34	0.22	0.10	0.08	0.12	0.18

Assume that the threshold design acceleration level that can be accepted by a particular design element (topside equipment or structural response) is $a_t=3.4 \text{ m/s}^2$ ($0.35g$, where g is the acceleration due to gravity). Applying the dynamic amplification provided in Table 1, and with $a_{WF}=1.6 \text{ m/s}^2$ and $a_{HFmax,m}= 5.2 \text{ m/s}^2$, it can be observed that a $r_{reqd}=k_p/k_m=26$ (Table 2) is sufficient to keep the maximum accelerations at the prototypes scale $a_{HFmax,p} < a_t$ for all the pulse periods. It is best to keep the stiffness ratios to a minimum to reduce the weight of the structural stiffening and also the cost. Tables 3 and 4 show the corresponding results for a half-sine pulse form (the details of which are provided in Vinayan and Zou 2014). For the same level of the threshold acceleration, the stiffness ratio obtained is $k_p/k_m=24$. From an engineering perspective, the difference between the stiffness ratios due to the pulse forms is not significant.

Table 2 Horizontal acceleration at prototype scale symmetric triangular pulse

k_p/k_m	Symmetrical Triangular Pulse				
	Pulse Period (s)				
	0.1	0.2	0.3	0.4	0.5
	$a_p \text{ (m/s}^2\text{)}$				
16	4.95	2.79	2.15	2.74	3.18
18	4.51	2.81	2.19	2.48	3.20
20	4.17	2.79	2.27	2.32	2.96
22	3.85	2.71	2.33	2.34	2.70
24	3.58	2.62	2.35	2.44	2.64
26	3.33	2.51	2.32	2.49	2.74
28	3.13	2.39	2.26	2.48	2.81
30	2.96	2.28	2.18	2.41	2.78
32	2.83	2.19	2.10	2.31	2.67
34	2.74	2.12	2.04	2.22	2.54

Table 3 Dynamic amplification factor for half-sine pulse

k_p/k_m	Half-sine Pulse				
	Pulse Period (s)				
	0.1	0.2	0.3	0.4	0.5
	a_p/a_m				
16	0.45	0.13	0.14	0.17	0.19
18	0.41	0.15	0.11	0.16	0.20
20	0.38	0.16	0.10	0.18	0.17
22	0.35	0.15	0.09	0.15	0.17
24	0.33	0.11	0.10	0.14	0.17
26	0.31	0.10	0.10	0.14	0.15
28	0.30	0.10	0.08	0.14	0.15
30	0.32	0.09	0.08	0.12	0.15
32	0.34	0.10	0.08	0.12	0.14
34	0.34	0.11	0.08	0.12	0.13

Table 4 Horizontal acceleration at prototype scale for half-sine pulse

k_p/k_m	Half-sine Pulse				
	Pulse Period (s)				
	0.1	0.2	0.3	0.4	0.5
	$a_p (m/s^2)$				
16	3.96	2.29	2.34	2.49	2.61
18	3.75	2.39	2.18	2.44	2.66
20	3.58	2.44	2.10	2.52	2.50
22	3.44	2.36	2.08	2.38	2.49
24	3.32	2.18	2.15	2.33	2.47
26	3.21	2.11	2.13	2.32	2.39
28	3.14	2.10	2.03	2.35	2.38
30	3.29	2.08	2.01	2.25	2.37
32	3.37	2.11	2.00	2.23	2.31
34	3.39	2.17	2.02	2.22	2.29

6. Conclusions

A typical dry-transport model test configuration is such that it is difficult to scale the prototype tie-down stiffness to model scale. The combination of the mass of the cargo and the relatively high tie-down stiffness results in system that has a natural period well within the pulse periods of typical wave-slamming events. Due to this, the measured loads and accelerations tend to have a HF ringing like behavior that is not a true representation of the actual scenario in prototype scale. The typical approaches taken to address this are:

- (1) Directly use the model test results without any correction for the HF response. This leads to conservative and impractical levels of accelerations and tie-down forces. For the case we studied in this paper, the measured horizontal acceleration is about 0.7 g which would be well above the design limit, say 0.35 g. With this approach, the only alternative is to avoid the high sea-states at which the design acceleration levels are exceeded. Weather avoidance causes unnecessary delays in the overall schedule and increases the transportation cost.
- (2) The other approach is to completely disregard the HF response and use the WF component only for design. For the case we studied in this paper, the measured wave-frequency horizontal acceleration is about 0.2 g which would be considerably underestimated if the ratio of prototype and model scale is 20 or less. This approach ignores an amplification of the response due to HF effects and can result in severe damage to the installed topsides/equipment and local hull structure and this in turn can result in major capital loss.

A correlation method has been developed here that addresses both these aspects. The underlying principle behind it is to utilize the measured results in a correct and consistent manner for designing tie-downs to ensure a safe and economic dry transportation.

In order to derive a robust solution, two impulsive pulse forms have been investigated. No major difference has been observed and triangular pulse form yields a slightly higher requirement of prototype tie-down stiffness. In addition, a set of steps are provided as guidance for optimizing the final tie down design to avoid unnecessary excessive high-frequency loading on topsides, hull and topsides connecting structures.

Acknowledgments

The author would like to acknowledge the management of Houston Offshore Engineering, an Atkins Company for supporting the Research and Development work on Dry Transport Analysis.

References

- Argate, S. (2013), *Hull slamming*, *Applied Mechanics Reviews*, **64**(6), 060803-1- 060803-35
- Bhattacharya, S. (2005), *Handbook of Offshore Engineering, Volumes 1-2*, (*“Offshore Installation, Chapter 14, Bader Diab and Naji Tahan*), Elsevier.
- Chopra, A.K. (1995), *Dynamics of Structures: Theory and Applications to Earthquake Engineering*, Prentice Hall.
- Hartog, J.P.D. (1985), *Mechanical Vibrations*, Dover.
- Isaacson, M. and Prasad, S. (1994), “Wave slamming on a horizontal circular cylinder”, *Int. J. Offshore Polar.*, **4**(2),
- Piersol, A.G. and Paez, T.L. (2010), *Harris’ Shock and Vibration Handbook*, 6th Ed., McGraw-Hill.
- Vinayan, V. and Zou, J. (2014). “Tie down stiffness effects on high-frequency response of cargo during dry transport”, *Proceedings of the 19th SNAME Offshore Symposium*, Houston, TX, February.
- Wirsching, P.H., Paez, T.L. and Ortiz, K. (2006), *Random Vibrations: Theory and Practice*, Dover.